Metrol. Meas. Syst., Vol. XXI (2014), No. 4, pp. 685–698.

PAN POLSKA AKADEMIA NAUK

METROLOGY AND MEASUREMENT SYSTEMS

Index 330930, ISSN 0860-8229

www.metrology.pg.gda.pl

M&MS

CHARACTERIZATION OF OPTICAL AND ELECTRICAL PROPERTIES OF TRANSPARENT CONDUCTIVE BORON-DOPED DIAMOND THIN FILMS GROWN ON FUSED SILICA

Robert Bogdanowicz

Dept. of Metrology and Optoelectronics, Faculty of Electronics, Telecommunications and Informatics, Gdansk University of Technology, 11/12 G. Narutowicza St., 80-233 Gdansk, Poland (✉ rbogdan@eti.pg.gda.pl, +48583471503)

Abstract

A conductive boron-doped diamond (BDD) grown on a fused silica/quartz has been investigated. Diamond thin films were deposited by the microwave plasma enhanced chemical vapor deposition (MW PECVD). The main parameters of the BDD synthesis, i.e. the methane admixture and the substrate temperature were investigated in detail. Preliminary studies of optical properties were performed to qualify an optimal CVD synthesis and film parameters for optical sensing applications. The SEM micro-images showed the homogenous, continuous and polycrystalline surface morphology; the mean grain size was within the range of 100-250 nm. The fabricated conductive boron-doped diamond thin films displayed the resistivity below 500 mOhm cm^{-1} and the transmittance over 50% in the VIS-NIR wavelength range. The studies of optical constants were performed using the spectroscopic ellipsometry for the wavelength range between 260 and 820 nm. A detailed error analysis of the ellipsometric system and optical modelling estimation has been provided. The refractive index values at the 550 nm wavelength were high and varied between 2.24 and 2.35 depending on the percentage content of methane and the temperature of deposition.

Keywords: *CVD, boron-doped diamond, optical properties, optical coatings, spectroscopic ellipsometry.*

1. Introduction

Diamond is a semiconductor with a wide energy band-gap of E_g = 5.45 eV, but when doped with boron it becomes a p-type semiconducting material with outstanding electronic properties. The main advantages of boron-doped diamond films are a high electron and hole mobility 4500 and 3800 $cm^2V^{-1}s^{-1}$, respectively, and the thermal conductivity 24 $Wcm^{-1}K^1$. In comparison to the most common semiconductor materials, such as silicon or gallium nitride, their properties are several times better [1]. Currently, diamond devices are used in high power electronics [2], diamond diodes [3], high-power switches [4] or high-frequency devices, such as transistors [5]. However, the most common use of BDD materials is for electrodes in electrochemistry [6–8] or spectroelectrochemistry [9]. The electrodes of this type have a good chemical and electrochemical stability even in highly aggressive media, a long lifetime and a wide potential window for the water discharge. They could be used effectively in electrochemical sensors [10, 11] designed for environment monitoring and biomedical applications [12, 13]. They also offer an extremely high detection sensitivity of $10^{-6} \div 10^{-9}$ M in case of bioanalytes (e.g. proteins [14] or DNA [15]), depending on deposition parameters and a medium. Apart from the aforementioned advantages we propose to apply boron-doped diamond as a sensing film in electrochemical sensors and fibre optic sensors [16, 17].

Article history: received on Jul. 22, 2014; accepted on Oct. 14, 2014; available online on Dec. 15, 2014; DOI: 10.2478/mms-2014-0059.

Reports on optical properties of thin diamond films can be found in the published literature. Remes *et al*. [18] investigated optical properties of an un-doped NCD film on fused silica by using the photo-thermal deflection spectroscopy, calorimetry and dual beam photocurrent spectroscopy. In the case of many applications, using a high temperature process is not acceptable, e.g. in coating of quartz or complementary metal oxide semiconductors. Kromka *et al.* [19] investigated an impact of the low-temperature MW CVD process on optical properties of nanocrystalline diamond films (NCD) on silicon and quartz substrates; the films displayed a transmittance of ca. 70% and a high refractive index of 2.34 at the 550 nm wavelength. Potocky et al. [20] showed a refractive index of 2.2 to 2.4 (@550 nm) on a quartz substrate for the growth temperature below 400 °C. Optical properties of diamond layers strongly depend on the deposition temperature [21, 22].

The work of Gupta *et al.* demonstrated an increasing influence of the boron dopant on optical and morphological properties of BDD [23]. They suggest that an area of the high conductivity density correlates with a high boron doping level along with electrical conductivity heterogeneity of boron-doped poly-/microcrystalline diamond surfaces. Stotter *et al.* [9] investigated an optical transmittance in the UV-VIS range and absorbance with a spectro-electrochemistry method based on measurements using an optical transparent BDD electrode with a maximum 50% transmittance on quartz. These results showed that the optical and electrical properties were extremely stable during 48-h exposure tests in various aqueous (HNO_3, NaOH) solutions and non-aqueous (e.g. chlorinated) solvents.

Gajewski *et al*. [24] investigated optical parameters, namely, the photocurrent and the optical absorption coefficient in un-doped and low-doped nano-crystalline diamond films deposited on monocrystalline silicon. The results of the spectrally resolved photocurrent and photo-thermal deflection spectroscopy in a low energy range, between 0.5 and 1.0 eV, confirmed that boron as well as sp^2 carbon phases in the grain boundaries govern the optical-absorption process.

Optical properties of a heavily-doped BDD film were studied by Zimmer *et al.* [25] with the spectroscopic ellipsometry. An NCD film was deposited on Si wafers at the mean dopant level [B]/[C] of 6500 ppm and with the complex index of refraction calculated from the Lorentz model. These films have well-defined optical properties: UV-visible refractive indexes close to those of recent un-doped and composite NCD films, unusual nonzero extinction coefficients due to a high boron sub-gap absorption present in IR.

However, there is still lack of information about optical constants of boron-doped diamond deposited on transparent substrates in the VIS-NIR region and their spectral dependence. These parameters are critical for developing integrated optical sensors [26, 27], transparent electronics [28] and opto-electrochemical bio-sensing devices [29, 30].

This paper provides the detailed information about the optical constants and transmittance of boron-doped diamond thin films deposited by MW PECVD on fused silica substrates. The influence of the main parameters of BDD synthesis, i.e. the methane admixture and the substrate temperature, was studied in detail. The surface morphology was assessed by the scanning electron microscopy (SEM). The resistivity of a BDD electrode was studied using four-point probe measurements. The thickness, optical energy band gap and optical constants of the fabricated diamond films were investigated in the VIS-NIR range by means of the spectroscopic ellipsometry.

2. Experimental

2.1. Deposition of boron-doped diamond films

The BDD films were synthesized in the MW PECVD system (SEKI Technotron, AX6300, Japan) on 10 x 10 mm quartz substrates. The substrates had been washed for 5 minutes in an ultrasonic bath using acetone and 2-isopropanol. Next, they had been seeded for 1 hour by sonication in a commercially available diamond suspension with a grain size of 5-20 nm (Blue-seeds, ITC, USA) [31, 32]. Then the substrates were washed again in 2-isopropanol and dried in a stream of nitrogen.

The deposition procedure was performed on a molybdenum stage heated to 500ºC and 700ºC. The base pressure was about 10^{-4} Torr and the process pressure was kept at 50 Torr. The molar ratio of CH_4:H_2 mixture was kept at 1% and 4% of the gas volume at 300 sccm of the total flow rate. The highly excited plasma was generated with a microwave radiation (2.45 GHz) and optimized for the diamond synthesis at a power of 1300 W [33–35]. All samples had been etched in pure H_2 plasma for 3 min, and then doped by using the diborane (B_2H_6) dopant precursor. The B/C ratio of samples was kept at 5000 ppm. The growth time of the polycrystalline film (see Table 1) was optimized to produce films of 400 ± 50 nm thickness [36].

Table 1. A set of diamond film samples, including the applied deposition parameters.

Sample	$[B]/[C]_{gas}$ (ppm)	Gas flow (sccm)	CH_4 (%)	Tc(°C)	Time (min)
BDD-1-500	5000	300	1%	500	60
BDD-1-700	5000	300	1%	700	60
BDD-4-500	5000	300	4%	500	30
BDD-4-700	5000	300	4%	700	30

The morphological studies were performed with a Hitachi S-3400N scanning electron microscope (SEM). The variable pressure SEM mode (VP-SEM) was used, which allows to make measurements regardless of the sample electrical conductivity. Moreover, the secondary electron mode was applied with a 20 kV accelerating voltage.

The resistivity of boron-doped diamond films was measured by a four-point probe system. The current value was gradually increased from 0 to 100 μA with a 10 μA step. A source meter (Keithley 2400, UK) was used as the current source applied to the external probes. The voltage on the internal probes was measured by a VA multimeter (Appa 207, Taiwan). Each sample was measured at four surface points. In cases when the film thickness is much smaller than the distance between the probes, the surface resistivity can be calculated from Eq. (1) [37]:

$$\rho = \frac{\pi}{\ln(2)} \cdot \frac{V}{I} \cdot h, \tag{1}$$

where V is the voltage measured on the internal probes, I is the current applied to the external probes, and h is the thickness of a layer.

2.2. Spectroscopic ellipsometry measurement system

The ellipsometry is an optical method for analyzing thin layers. It is based on the polarization state measurement of the light beam reflected from a sample. Such a procedure is used for thickness monitoring of dielectric and semiconductor layers synthesized during PVD or CVD processes. However, the described procedure had been adapted with respect to that of Tompkins *et al.* [38], particularly in examination of the measurement data, theoretical modelling and fitting.

The linearly polarized light beam is incident on a sample at ϕ_0=70° angle, where the layer thickness is d_1. N_0 is the refractive index of ambient, where substrate is located. A thin diamond film covers the substrate characterized by the refractive index N_2. The complex refractive indices of investigated layers are denoted as N_1. For ellipsometric purposes the complex-amplitude parameter ρ is defined as the ratio of total reflection coefficients:

$$\rho = \frac{r^p}{r^s} = \tan\Psi\, e^{\,j\Delta}. \tag{2}$$

The ellipsometric angles Δ and Ψ represent the amplitude and phase ratio difference between the p- and s-polarization of the light beam [12]. The amplitude reflectance coefficients in both polarization modes are expressed as follows:

$$\frac{r^p}{r^s} = \left[\frac{r_{01}^p + r_{12}^p \exp\left(-j2\beta_1\right)}{1 + r_{01}^p r_{12}^p \exp\left(-j2\beta_1\right)}\right] \Big/ \left[\frac{r_{01}^s + r_{12}^s \exp\left(-j2\beta_1\right)}{1 + r_{01}^s r_{12}^s \exp\left(-j2\beta_1\right)}\right], \tag{3}$$

where r_{01}, r_{12} are the Fresnel reflection coefficients defined at boundaries of various *i*-media, which depend on the $N_i = n_i - ik_i$ complex refractive index [14]. The phase shift due to the light beam refraction of angle ϕ_1 is expressed by:

$$\beta_i = 4\pi\left(\frac{d_i}{\lambda}\right) N_i \cos\phi_i. \tag{4}$$

The refractive indices N_0, N_1 and N_2 are complex functions of the λ wavelength of the incident light beam. The substitution of Fresnel reflection coefficients and Eqs. (3)-(4) in Eq. (2) gives the complex ratio ρ as a function of the medium refractive indices, light wavelength and layer thicknesses.

The first step of the ellipsometric analysis is an assumption of a model using a number of layers and layer types. The introductory parameterization of optical indices of each layer is necessary to calculate angles Δ and Ψ using the formulas (2)-(4) (see Fig. 1). The last step of the data investigation is fitting the model to the experimental results. The selection of a suitable optical model is the most important step of analysis.

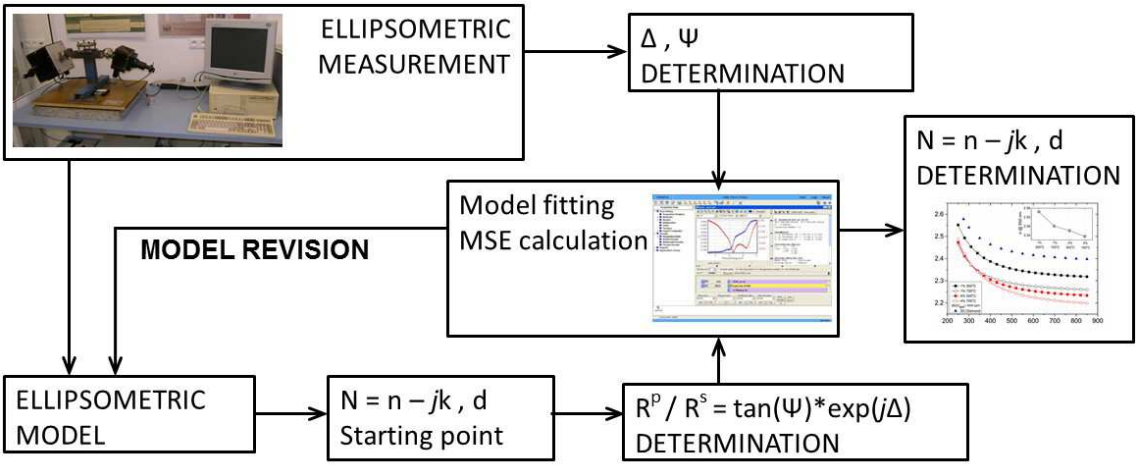

Fig. 1. The scheme of the ellipsometric measurement algorithm.

The spectroscopic ellipsometry investigations were carried out with a Jobin-Yvon UVISEL phase-modulated ellipsometer (HORIBA Jobin-Yvon Inc., Edison, USA). The investigated wavelength region was between 250 and 800 nm, with a step of less than 0.5 nm. The experiments were carried out at a room temperature using the angle of incidence fixed at 70° and the compensator set at 45°. The incidence angle resulted from the Brewster's angle of quartz substrate. The DeltaPsi software (v. 2.4.3) was employed to determine the spectral distributions of the refractive index n (λ) and the extinction coefficient k (λ) of the obtained diamond films. The relative sp^3/sp^2 phase ratios were estimated by fitting a diamond film using the Bruggeman effective medium approximation (BEMA). To estimate this ratios, the BDD thin films were considered as heterogeneous material consisting of diamond (sp^3) and graphitic phases (sp^2), giving optical parameters estimated by the BEMA [38, 39], expressed by:

$$\frac{<\varepsilon>-\varepsilon_h}{<\varepsilon>+\varepsilon_h}=\sum_j f_j \frac{\varepsilon_j-\varepsilon_h}{\varepsilon_j+\gamma\varepsilon_h}, \tag{5}$$

where ε is the dielectric function of the effective medium, ε_h is the dielectric function of the host, f_j is the fraction of the j_{th} constituent, and γ is a factor related to the screening and the shape of the inclusions (for example, $\gamma = 2$ for 3-dimensional spheres).

The efficient error-based figure of merit is crucial to know whether the assumed model fits the experiments. As the fitting measure the mean square error (MSE) was utilized [12], which is given by:

$$MSE=\frac{1}{2N-M}\sum_{i=1}^{N}\left[\left(\frac{\Psi_i^{\text{mod}}-\Psi_i^{\text{exp}}}{\sigma_{\Psi,i}^{\text{exp}}}\right)^2+\left(\frac{\Delta_i^{\text{mod}}-\Delta_i^{\text{exp}}}{\sigma_{\Delta,i}^{\text{exp}}}\right)^2\right]. \tag{6}$$

In Eq. (6) $\Delta^{\text{exp}}_{\text{i}}$, $\Delta^{\text{mod}}_{\text{i}}$, $\Psi^{\text{exp}}_{\text{i}}$, $\Psi^{\text{mod}}_{\text{i}}$ and σ_{i} represent the investigated, calculated and standard deviations for the data set i, while N is the number of measurement points and M is the number of fitted parameters.

The ellipsometric fitting was based here on a four-phase optical model (air/surface roughness film (SRL)/ diamond/ Si-wafer). The dispersion of Si <100> was taken from the database [40]. The dielectric function of the SRL was estimated using the BEMA. The

dispersion of quartz was taken from the database [41]. The assumption was made that a diamond film is an isotropic, homogeneous material; its dispersion being fitted by the Tauc-Lorentz oscillator (TL) model. This model has been recently used by Gioti *et al.* [42] and Logothetidis *et al.* [43] for amorphous semiconductors. The TL dispersion model is also widely used for modelling the optical dispersion of a-C, a-C: H [44] as well as polycrystalline diamond films [45]. The model is a combination of the Tauc joint density of states [42] and the quantum-mechanical Lorentz oscillator model [46]. The TL model fits to the dielectric functions of a class of an amorphous material. Such materials exhibit a peculiarity due to the presence of two separated contributions of the inter-band electronic transition related to an sp^2- and sp^3-bonded carbon [47]. The parameters of the TL model were estimated for each of the analysed films. Finally, the assumed optical model was fitted to the experimental data using the non-linear Levenberg-Marquardt regression method for the mean-square error minimization (MSE) [48].

3. Results

3.1. Surface morphology of boron-doped diamond

The morphology of boron-doped diamond layers grown on fused silica deposited at different temperatures and methane concentrations are presented in Figure 2. High crystallographic diamond films with a different surface morphology were obtained at a moderate temperature (550 °C to 700 °C) and methane concentration (1 or 4%). The low magnification images (1000x – insets Fig. 2.) show that the surfaces of all samples were fully covered by diamond crystals. Micro-cracks were observed in some areas of the deposited films. Those micro-cracks could be explained by a difference of the thermal expansion coefficient between the diamond and substrate that occurs as a stress on the surface of quartz during cooling (20ºC min^{-1}). Furthermore, these micro-cracks exhibit a slight impact on optical and electronic properties (see Section 3.3). The work of Gicquel *et al.* [49] shows comparable results and a high influence of the temperature and methane concentration on the quality of diamond films.

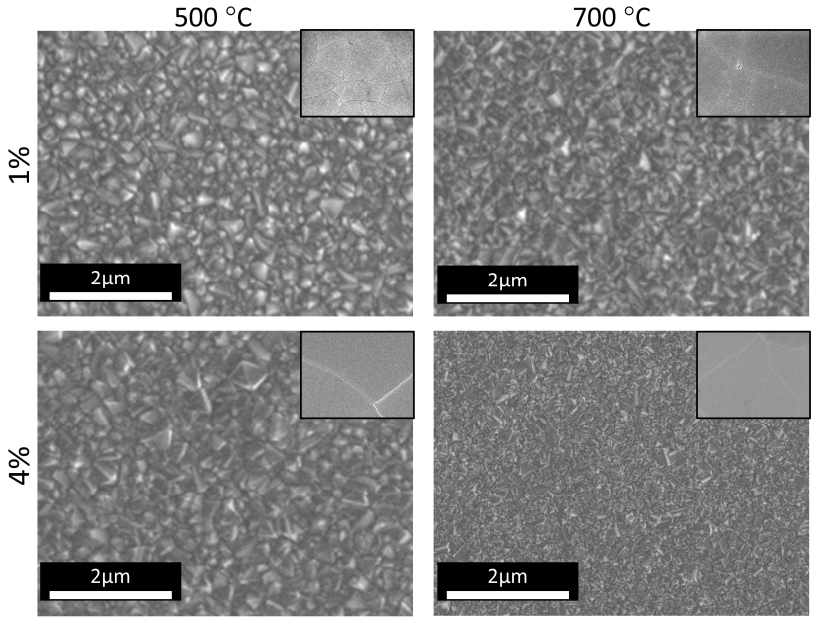

Fig. 2. The morphology of boron-doped diamond thin films on a quartz substrate as a function of the stage temperature and methane concentration ratio in the gas flow.

In case of the substrate temperature of 500 °C, there is no difference in grain size or homogeneity for the BDD-1-500 and BDD-4-500 samples. An average diameter of the grain is close to 250 nm. The surface morphology, homogeneity and diameter of the grain size for the BBD-1-700 sample is comparable to samples grown at 500°C. The change of the methane concentration from 1% to 4% for the substrate temperature 700°C has the most significant impact on the grain size, giving values below 100 nm.

3.2. Electrical parameters of BDD films

The electrical properties of BDD films were measured by a four-point probe system. The average conductivity and resistivity of deposited samples are listed in Table 2. The obtained resistivity values ranged between 35 and 0.02 Ω cm, which is in agreement with previous results [50, 51]. The lowest resistivity of about 20 mΩ cm was observed for the BDD-4-700 sample. The highest resistivity, i.e. 35 Ω cm, was achieved for the BDD-1-500 sample. It could be summarized, that the resistivity variations come mostly from the substrate temperature causing structure defects and carrier transport disturbances [52]. Moreover, the resistivity decreases with increasing the methane admixture in plasma. The 4% methane samples show a smaller amount of defects and micro-cracks, because films exhibit a smaller sp^3/sp^2 ratio introducing a lower stress in the structure [53].

Table 2. The electrical parameters of boron-doped diamond films deposited on fused silica substrates.

Sample	Rsh (Ω cm)	E_{gopt} (eV)
BDD-1-500	34.9	4.0
BDD-1-700	0.42	4.2
BDD-4-500	10.4	3.8
BDD-4-700	0.02	3.7

The optical band gap E_{gopt} was determined from the absorption coefficient α by using the Tauc plot [54]. The Tauc plot analysis indicates that band-to-band indirect transitions are more probable than the direct transitions. Therefore, the band gap values were estimated by extrapolating the linear portion of the $(\alpha h\nu)^{1/2}$ vs. $h\nu$ plot, where $h\nu$ is the photon energy, to $(\alpha h\nu)^{1/2}=0$. This conclusion was also supported by the results reported by Lee *et al.* [55], Hu *et al.* [56] or Taylor *et al.* [57].

In this study the band gap decreases from 4.2 eV estimated at the BDD-1-700 sample down to 4.01 eV and 3.7 eV achieved for the BDD-1-500 and the BDD-4-700 samples, respectively. Comparable band gap values have been reported by Hu *et al.* [56] or Zimmer *et al.* [58]. This fact is also correlated with a higher refractive index (see Fig. 3A), indicating the film densification [59]. It is worth of noting, that the optical band gap and optical constants are in agreement with a smooth surface nanostructure and a high sp^3 phase content [60].

3.3. Optical properties of boron-doped diamond grown on fused silica

The spectroscopic ellipsometry (SE) was employed to investigate the optical constants of the deposited diamond films. The refractive index n and the extinction coefficient k were calculated using an optical model, and later plotted as a function of the wavelength. The spectral variability of optical constants in samples with different methane admixtures and substrate temperatures are presented in Figure 3 (A and B).

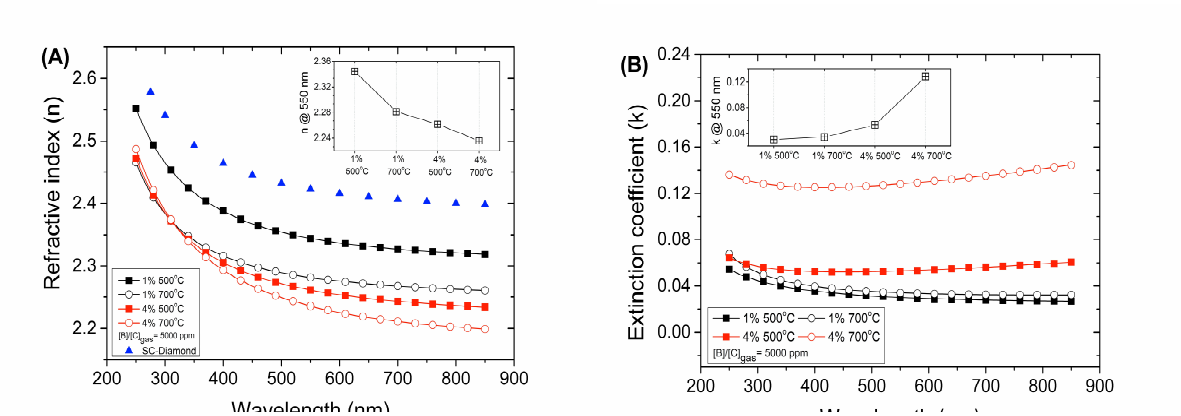

Fig. 3. Wavelength-dependent variability of (A) the refractive index n and (B) the extinction coefficient k in boron-doped diamond films deposited under various conditions related to the methane admixture and the substrate temperature. For comparative purposes, the refractive index measurements for a single-crystal diamond are shown (▲-SCD) [41]. Insets: the variability of n and k measured at 550 nm.

All deposited diamond films were characterized by a normal dispersion. The optical constants of BDD films decreased with increasing of the wavelength, exhibiting a typical behaviour near the band gap of the electronic transition. The refractive index of BDD films slightly decreased with increasing of the methane percentage and increasing of the deposition temperature. Nevertheless, the measured values were smaller than those for the single-crystal diamond reported by Palik [41]. This finding shows a smaller optical density of boron-doped diamond films.

The observed influence of an increasing methane content on the sample optical properties is evident. The refractive index varied between 2.24 and 2.35 for different methane contents and deposition temperatures at the 550 nm wavelength (see Inset of Fig. 3A). The obtained values were smaller than those for the single-crystal diamond (2.41), which is related to a decrease in the sp^3/sp^2 carbon phase ratio [53]. Most likely, the diamond film samples contained more defects and some nanocrystals, as demonstrated by SEM images (see Fig. 2).

In the case of the 1% methane content, the extinction coefficient was approximately 0.04, resulting in a high transparency of the boron-doped diamond samples. The extinction coefficients at 550 nm of samples produced at the 4% methane content reached 0.05 and 0.13 for the substrate temperatures of 500ºC and 700ºC, respectively. Moreover, the extinction coefficient increased with increasing a wavelength in the wavelength region above 350 nm. This can be explained by a higher sp^2 bond content and intensive boron incorporation between the grains [61] (see Table 3.).

The effect of a high k in the wavelength region above 350 nm was even pronounced in the case of overheated quartz substrates (i.e. 700ºC at 4% vol. of CH_4). Thus, the effect of the substrate temperature is discussable. Nevertheless, the boron induces an acceptor level at 0.37 eV (3450 nm) leading to an increased light absorption for higher energy levels. The Lorentz oscillator fitting shows the peak position near this value. It is noteworthy that the k value of

the BDD film produced at the 1.0% methane content and 500ºC is minimal, as illustrated by the inset in Fig. 3B. An increase in *k* values is correlated with the non-diamond phases in a nanocrystalline structure compared to that of a microcrystalline structure [62].

Table 1 lists the effective thicknesses of the BDD layer, SRL and the sp^3/sp^2 BEMA ratio estimated in ellipsometric measurements. Moreover, the *MSE* values of fits are showed there for comparison.

Table 3. The thickness of the BDD films and SRL, sp^3/sp^2 BEMA ratio and MSE values of the fits estimated from the spectroscopic ellipsometry.

Sample	Thickness (nm)	Growth rate (nm min^{-1})	SRL (nm)	sp^3/sp^2 BEMA ratio	MSE *(a.u.)*
BDD-1-500	400±2.6	6.66±0.04	15±0.3	2.1	5.3
BDD-1-700	396±2	6.6±0.03	18±0.2	1.8	3.8
BDD-4-500	483±4	16.1±0.06	16±0.5	0.8	9.5
BDD-4-700	360±3	12±0.05	16±0.4	0.3	7.2

The methane flow level increases meaningfully the growth rate of the BDD films. A shift from 1% up to 4 % of the methane admixture almost doubles the growth rate. The growth rate ranges from 6.6 nm min^{-1} to 16.1 nm min^{-1} for the BDD-1-500 and the BDD-4-500, respectively. We have obtained very similar roughness distributions of *ca.* 17 nm, given by SRL values, over the studied samples. These results are in agreement with previous findings described by Lee *et al.* [59].

A decrease of the sp^3/sp^2 ratios, estimated using the BEMA calculation, follows an increase of the methane admixture. Comparable trends were reported for BDD films grown on silicon wafer substrates by Gicquel *et al.* [49] and Stoner *et al.* [62].

The corresponding mean square error (MSE) achieved during the SE estimation is slightly smaller for the BDD-1-500 and BDD-1-700 samples, comparing to that of the BDD-4-500 and BDD-4-700 ones. Nevertheless, the MSE values of the BDD-4-500 and BDD-4-700 are still below 10, i.e. at the acceptable level [38].

The optical transmittance values measured for the films deposited on transparent quartz substrates are illustrated in Figure 4. In addition, photos of the corresponding samples were inset in the plot for illustrative purposes.

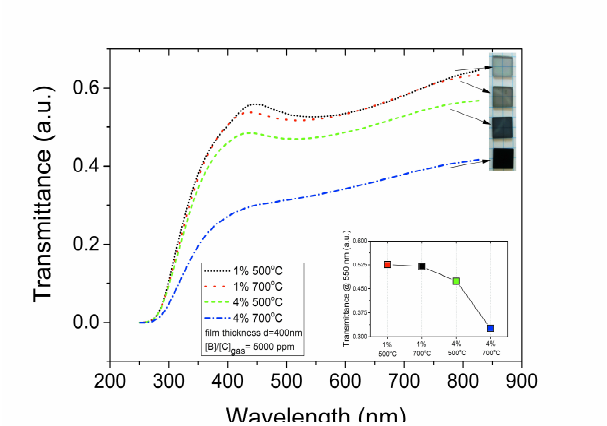

Fig. 4. The transmittance of boron-doped diamond films deposited on transparent quartz substrates under various conditions related to the methane admixture and the substrate temperature. The film thickness for each sample is also given. Inset: the variability of transmittance measured at 550 nm and photos of the presented BDD samples.

The transmittance of the BD-1-500/BD-1-700 and BD-4-500 samples reached over 50% in the VIS-NIR range. The transmittance values correspond directly with the sp^3/sp^2 ratio (see Table 3.). The transmittance values are sufficiently high with regard to a possible application of the films in optical sensing [63]. The BD-4-700 sample was very opaque, with the transmittance of about 30% and a low sp^3/sp^2 ratio. This characteristics was caused by an abundance of the sp^2/"cauliflower" [53] structure during the early stage of film growth. The transmittance can be further optimized by adjusting the methane content and the temperature level during the deposition process.

4. Conclusions

In summary, the BDD films were synthesized on quartz substrates using the MW PECVD method. The SEM micro-images showed the homogenous, continuous and polycrystalline surface morphology; the mean grain size was within the range of 100-250 nm. The fabricated conductive boron-doped diamond thin films displayed the resistivity below 500 mOhm cm^{-1} and the transmittance over 50% in the VIS-NIR wavelength range. The sp^3/sp^2 ratio investigation has shown that the substrate temperature equal to 500°C provided much better conditions for the diamond film deposition on fused silica than that equal to 700°C. Moreover, for the substrate temperature equal to 500°C the efficiency of boron building into the diamond lattice was higher for the methane content of 4%. The synthesized diamond films have been assumed to be an isotropic, homogeneous material, and their dispersion was fitted to the Tauc-Lorentz oscillator (TL) model. The refractive index values at the 550 nm wavelength were high and varied between 2.24 and 2.35 depending on the percentage content of methane and the temperature of deposition. The achieved parameters are critical for developing integrated optical sensors or opto-electrochemical bio-sensing devices.

Acknowledgements

This work was supported by the Polish National Science Centre (NCN) under the grant No. 2011/03/D/ST7/03541. The DS funds of the Faculty of Electronics, Telecommunications and Informatics at the Gdansk University of Technology are also acknowledged.

References

[1] Wort, C. J. H., & Balmer, R. S. (2008). Diamond as an electronic material. *Materials Today*, *11*(1–2), 22–28.

[2] Suzuki, M., Koizumi, S., Katagiri, M., Yoshida, H., Sakuma, N., Ono, T., & Sakai, T. (2004). Electrical characterization of phosphorus-doped n-type homoepitaxial diamond layers. *Diamond and Related Materials*, *13*(11–12), 2037–2040.

[3] Isberg, J., Hammersberg, J., Johansson, E., Wikström, T., Twitchen, D. J., Whitehead, A. J., Scarsbrook, G. A. (2002). High Carrier Mobility in Single-Crystal Plasma-Deposited Diamond. *Science*, *297*(5587), 1670–1672.

[4] Adamschik, M., Kusterer, J., Schmid, P., Schad, K. B., Grobe, D., Flöter, A., & Kohn, E. (2002). Diamond microwave micro relay. *Diamond and Related Materials*, *11*(3–6), 672–676.

[5] Petržela, J., Vyskočil, P., & Prokopec, J. (2010). Fundamental oscillators based on diamond transistors. In *Radioelektronika (RADIOELEKTRONIKA), 2010. 20th International Conference,* 1–4. Presented at the Radioelektronika (RADIOELEKTRONIKA), 2010 20th International Conference.

[6] Iniesta, J., Michaud, P. A., Panizza1, M., Cerisola1, G., Aldaz1, A., & Comninellis, C. (2001). Electrochemical oxidation of phenol at boron-doped diamond electrode. *Electrochimica Acta*, *46*(23), 3573–3578.

[7] Panizza, M., Michaud, P. A., Cerisola, G., & Comninellis, C. (2001). Electrochemical treatment of wastewaters containing organic pollutants on boron-doped diamond electrodes: Prediction of specific energy consumption and required electrode area. *Electrochemistry Communications*, *3*(7), 336–339.

[8] Brillas, E., Boye, B., Sirés, I., Garrido, J. A., Rodríguez, R. M., Arias, C., … Comninellis, C. (2004). Electrochemical destruction of chlorophenoxy herbicides by anodic oxidation and electro-Fenton using a boron-doped diamond electrode. *Electrochimica Acta*, *49*(25), 4487–4496.

[9] Stotter, J., Zak, J., Behler, Z., Show, Y., & Swain, G. M. (2002). Optical and Electrochemical Properties of Optically Transparent, Boron-Doped Diamond Thin Films Deposited on Quartz. *Analytical Chemistry*, *74*(23), 5924–5930.

[10] Bogdanowicz, R., Czupryniak, J., Gnyba, M., Ryl, J., Ossowski, T., Sobaszek, M., Darowicki, K. (2013). Amperometric sensing of chemical oxygen demand at glassy carbon and silicon electrodes modified with boron-doped diamond. *Sensors and Actuators B: Chemical*, *189*, 30–36.

[11] Bogdanowicz, R. (2013). Influence of the boron doping level on the electrochemical oxidation of the azo dyes at Si/BDD thin film electrodes. *Diamond and Related Materials*, (39), 82–88.

[12] Nebel, C. E., Rezek, B., Shin, D., Uetsuka, H., & Yang, N. (2007). Diamond for bio-sensor applications. *Journal of Physics D: Applied Physics*, *40*(20), 6443.

[13] Weng, J., Zhang, J., Li, H., Sun, L., Lin, C., & Zhang, Q. (2008). Label-Free DNA Sensor by Boron-Doped Diamond Electrode Using an ac Impedimetric Approach. *Analytical Chemistry*, *80*(18), 7075–7083.

[14] Trouillon, R., & O'Hare, D. (2010). Comparison of glassy carbon and boron doped diamond electrodes: Resistance to biofouling. *Electrochimica Acta*, *55*(22), 6586–6595.

[15] Weng, J., Zhang, J., Li, H., Sun, L., Lin, C., & Zhang, Q. (2008). Label-Free DNA Sensor by Boron-Doped Diamond Electrode Using an ac Impedimetric Approach. *Analytical Chemistry*, *80*(18), 7075–7083.

[16] Bogdanowicz, R., Śmietana, M., Gnyba, M., Ficek, M., Straňák, V., Goluński, Ł., Ryl, J. (2013). Nucleation and growth of CVD diamond on fused silica optical fibres with titanium dioxide interlayer. *physica status solidi (a)*, *210*(10), 1991–1997.

[17] Smietana, M., Szmidt, J., Dudek, M., & Niedzielski, P. (2004). Optical properties of diamond-like cladding for optical fibres. *Diamond and Related Materials*, *13*(4–8), 954–957.

[18] Remes, Z. (2010). High optical quality nanocrystalline diamond with reduced non-diamond contamination. *Diamond and Related Materials*, (19), 453–456.

[19] Kromka, A., Rezek, B., Remes, Z., Michalka, M., Ledinsky, M., Zemek, J., Vanecek, M. (2008). Formation of Continuous Nanocrystalline Diamond Layers on Glass and Silicon at Low Temperatures. *Chemical Vapor Deposition*, *14*(7-8), 181–186.

[20] Potocky, S., Kromka, A., Potmesil, J., Remes, Z., Vorlicek, V., Vanecek, M., & Michalka, M. (2007). Investigation of nanocrystalline diamond films grown on silicon and glass at substrate temperature below 400 °C. *Diamond and Related Materials*, *16,* (4–7), 744–747.

[21] Hu, Z. G., & Hess, P. (2006). Optical constants and thermo-optic coefficients of nanocrystalline diamond films at 30–500 °C. *Applied Physics Letters*, *89*(8), 081906–081906–3.

[22] Hu, Z. G., Prunici, P., Hess, P., & Chen, K. H. (2007). Optical properties of nanocrystalline diamond films from mid-infrared to ultraviolet using reflectometry and ellipsometry. *Journal of Materials Science: Materials in Electronics*, *18*(1), 37–41.

[23] Gupta, S., Dudipala, A., Williams, O. A., Haenen, K., & Bohannan, E. (2008). Ex situ variable angle spectroscopic ellipsometry studies on chemical vapor deposited boron-doped diamond films: Layered structure and modeling aspects. *Journal of Applied Physics*, *104*(7), 073514.

[24] Gajewski, W., Achatz, P., Williams, O. A., Haenen, K., Bustarret, E., Stutzmann, M., & Garrido, J. A. (2009). Electronic and optical properties of boron-doped nanocrystalline diamond films. *Physical Review B*, *79*(4), 045206.

[25] Zimmer, A., Williams, O. A., Haenen, K., & Terryn, H. (2008). Optical properties of heavily boron-doped nanocrystalline diamond films studied by spectroscopic ellipsometry. *Applied Physics Letters*, *93*(13), 131910–131910–3.

[26] Bogdanowicz, R., Śmietana, M., Gnyba, M., Ficek, M., Straňák, V., Goluński, Ł., Ryl, J. (2013). Nucleation and growth of CVD diamond on fused silica optical fibres with titanium dioxide interlayer. *physica status solidi (a)*, *210*(10), 1991–1997.

[27] Smietana, M., Szmidt, J., Dudek, M., & Niedzielski, P. (2004). Optical properties of diamond-like cladding for optical fibres. *Diamond and Related Materials*, *13*(4–8), 954–957.

[28] Daenen, M., Williams, O. A., D'Haen, J., Haenen, K., & Nesládek, M. (2006). Seeding, growth and characterization of nanocrystalline diamond films on various substrates. *physica status solidi (a)*, *203*(12), 3005–3010.

[29] Stotter, J., Show, Y., Wang, S., & Swain, G. (2005). Comparison of the Electrical, Optical, and Electrochemical Properties of Diamond and Indium Tin Oxide Thin-Film Electrodes. *Chemistry of Materials*, *17*(19), 4880–4888.

[30] Stotter, J., Zak, J., Behler, Z., Show, Y., & Swain, G. M. (2002). Optical and Electrochemical Properties of Optically Transparent, Boron-Doped Diamond Thin Films Deposited on Quartz. *Analytical Chemistry*, *74*(23), 5924–5930.

[31] Kromka, A., Rezek, B., Kalbacova, M., Baresova, V., Zemek, J., Konak, C., & Vanecek, M. (2009). Diamond Seeding and Growth of Hierarchically Structured Films for Tissue Engineering. *Advanced Engineering Materials*, *11*(7), B71–B76.

[32] Shenderova, O., Hens, S., & McGuire, G. (2010). Seeding slurries based on detonation nanodiamond in DMSO. *Diamond and Related Materials*, *19*(2–3), 260–267.

[33] Bogdanowicz, R., Gnyba, M., & Wroczyński, P. (2006). Optoelectronic monitoring of plasma discharge optimized for thin diamond film synthesis. *Journal de Physique IV (Proceedings)*, *137*, 57–60.

[34] Bogdanowicz, R., Gnyba, M., Wroczynski, P., & Kosmowski, B. B. (n.d.). Optoelectronic system for monitoring of thin diamond layers growth. *Journal of optoelectronics and advanced materials*, *12*(8), 1660–1665. Retrieved from http://cat.inist.fr/?aModele=afficheN&cpsidt=23110414

[35] Bogdanowicz, R. (2008). Investigation of H2:CH4 Plasma Composition by Means of Spatially Resolved Optical Spectroscopy. *Acta Phys. Pol.*, A33–A38.

[36] Kraszewski, M., & Bogdanowicz, R. (2013). Laser Reflectance Interferometry System with a 405 Nm Laser Diode for in Situ Measurements of CVD Diamond Thickness. *Metrology and Measurement Systems*, *20*(4), 543–554.

[37] Sze, S. M., & Ng, K. K. (2006). *Physics of Semiconductor Devices*. John Wiley & Sons.

[38] Tompkins, H., & Irene, E. A. (2005). *Handbook of Ellipsometry*. William Andrew.

[39] Khardani, M., Bouaïcha, M., & Bessaïs, B. (2007). Bruggeman effective medium approach for modelling optical properties of porous silicon: comparison with experiment. *physica status solidi (c)*, *4*(6), 1986–1990.

[40] Palik, E. D. (Ed.). (1991). *Handbook of Optical Constants of Solids, 2* (1st ed.). Academic Press.

[41] Palik, E. D. (1998). *Handbook of Optical Constants of Solids*. Academic Press.

[42] Gioti, M., Papadimitriou, D., & Logothetidis, S. (2000). Optical properties and new vibrational modes in carbon films. *Diamond and Related Materials*, *9*(3–6), 741–745.

[43] Logothetidis, S., Gioti, M., Patsalas, P., & Charitidis, C. (1999). Insights on the deposition mechanism of sputtered amorphous carbon films. *Carbon*, *37*(5), 765–769.

[44] Jellison Jr., G. E., Merkulov, V. I., Puretzky, A. A., Geohegan, D. B., Eres, G., Lowndes, D. H., Caughman, J. B. (2000). Characterization of thin-film amorphous semiconductors using spectroscopic ellipsometry. *Thin Solid Films*, *377–378*, 68–73.

[45] Majumdar, A., Schäfer, J., Mishra, P., Ghose, D., Meichsner, J., & Hippler, R. (2007). Chemical composition and bond structure of carbon-nitride films deposited by CH4/N2 dielectric barrier discharge. *Surface and Coatings Technology*, *201*(14), 6437–6444.

[46] Gioti, M., Logothetidis, S. (2003). Dielectric function, electronic properties and optical constants of amorphous carbon and carbon nitride films. *Diamond and Related Materials*, *12*(3–7), 957–962.

[47] Jellison, G. E., J., & Modine, F. A. (1996). Parameterization of the optical functions of amorphous materials in the interband region. *Applied Physics Letters*, *69*(3), 371–373.

[48] Tompkins, H., & Irene, E. A. (2005). *Handbook of Ellipsometry*. William Andrew.

[49] Gicquel, A., Hassouni, K., Silva, F., & Achard, J. (2001). CVD diamond films: from growth to applications. *Current Applied Physics*, *1*(6), 479–496.

[50] Lagrange, J.-P., Deneuville, A., & Gheeraert, E. (1999). A large range of boron doping with low compensation ratio for homoepitaxial diamond films. *Carbon*, *37*(5), 807–810.

[51] Werner, M., Job, R., Zaitzev, A., Fahrner, W. R., Seifert, W., Johnston, C., Chalker, P. R. (1996). The Relationship between Resistivity and Boron Doping Concentration of Single and Polycrystalline Diamond. *physica status solidi (a)*, *154*(1), 385–393.

[52] Nesládek, M., Tromson, D., Mer, C., Bergonzo, P., Hubik, P., & Mares, J. J. (2006). Superconductive B-doped nanocrystalline diamond thin films: Electrical transport and Raman spectra. *Applied Physics Letters*, *88*(23), 232111.

[53] May, P. W., Ludlow, W. J., Hannaway, M., Heard, P. J., Smith, J. A., & Rosser, K. N. (2008). Raman and conductivity studies of boron-doped microcrystalline diamond, facetted nanocrystalline diamond and cauliflower diamond films. *Diamond and Related Materials*, *17*(2), 105–117.

[54] Lewkowicz, A., Synak, A., Grobelna, B., Bojarski, P., Bogdanowicz, R., Karczewski, J., Behrendt, M. (2014). Thickness and structure change of titanium(IV) oxide thin films synthesized by the sol–gel spin coating method. *Optical Materials*, *36*(10), 1739–1744.

[55] Lee, H., Kim, I.-Y., Han, S.-S., Bae, B.-S., Choi, M. K., & Yang, I.-S. (2001). Spectroscopic ellipsometry and Raman study of fluorinated nanocrystalline carbon thin films. *Journal of Applied Physics*, *90*(2), 813–818.

[56] Hu, Z. G., Prunici, P., Hess, P., & Chen, K. H. (2007). Optical properties of nanocrystalline diamond films from mid-infrared to ultraviolet using reflectometry and ellipsometry. *Journal of Materials Science: Materials in Electronics*, *18*(1), 37–41.

[57] Taylor, A., Fekete, L., Hubík, P., Jäger, A., Janíček, P., Mortet, V., … Vacík, J. (2014). Large area deposition of boron doped nano-crystalline diamond films at low temperatures using microwave plasma enhanced chemical vapour deposition with linear antenna delivery. *Diamond and Related Materials*, *47*, 27–34.

[58] Zimmer, A., Williams, O. A., Haenen, K., Terryn, H. (2008). Optical properties of heavily boron-doped nanocrystalline diamond films studied by spectroscopic ellipsometry. *Applied Physics Letters*, *93*(13), 131910–131910–3.

[59] Lee, S.-T., Lin, Z., Jiang, X. (1999). CVD diamond films: nucleation and growth. *Materials Science and Engineering: R: Reports*, *25*(4), 123–154.

[60] Asmussen, J., Reinhard, D. (2002). *Diamond Films Handbook*. CRC Press.

[61] Turner, S., Lu, Y.-G., Janssens, S. D., Pieve, F. D., Lamoen, D., Verbeeck, J., Tendeloo, G. V. (2012). Local boron environment in B-doped nanocrystalline diamond films. *Nanoscale*, *4*(19), 5960–5964.

[62] Stoner, B. r., Williams, B. e., Wolter, S. d., Nishimura, K., Glass, J. t. (1992). In situ growth rate measurement and nucleation enhancement for microwave plasma CVD of diamond. *Journal of Materials Research*, *7*(02), 257–260.

[63] Arregui, F. J. (2010). *Sensors Based on Nanostructured Materials*. Springer.